X-651-64-358

NASA TM X-55157

DETAILED BEHAVIOR

OF THE

MIDLATITUDE IONOSPHERE

FROM THE

EXPLORER XVII SATELLITE

NOVEMBER 1964

DETAILED BEHAVIOR OF THE MIDLATITUDE IONOSPHERE

FROM THE EXPLORER XVII SATELLITE

by

L. H. Brace and N. W. Spencer
Goddard Space Flight Center
Greenbelt, Maryland

and

A. Dalgarno
The Queen's University of Belfast,
N. Ireland

ABSTRACT

Measurements of electron temperature and ion density by electrostatic probes on the Explorer 17 satellite have revealed the detailed diurnal and latitudinal behavior of the summer ionosphere near the altitude of the F_2 maximum over the eastern United States at the time of solar minimum. The electron temperature at 40° North magnetic latitude is observed to rise rapidly from a nighttime value of about 1100°K to a mid-morning maximum of 2700°K followed by an afternoon plateau of 2000°K. The electron temperature always exceeds accepted values of neutral gas temperature and thus reflects the existence of heat sources in both the daytime and nocturnal ionosphere. The ion density displays a maximum value about three hours after local noon. A strong degree of latitude control, evident near the F_2 maximum, causes the temperature to increase and the density to decrease with increasing latitude. The electron temperature is relatively independent of altitude between 260 and 450 kilometers in the forenoon but displays a slight increase with altitude at night. The diurnal variations found over stations at 10° and 60° North magnetic latitude display general characteristics similar to those found at 40° N and also reveal the inverse gradients of temperature and density with latitude. Calculations based on the measurements show that the ion temperature begins to exceed the neutral temperature significantly above 300 kilometers and approaches the electron temperature near 600 km. The ratio of electron to ion temperature at 300 km is between 2 and 3 in the daytime and about 1.5, but highly variable, at night. The measurements are also employed to calculate the amount of electron heating in the F region. It appears that heating by solar ultraviolet radiation is adequate to explain the daytime results below 300 kilometers, and that the available flux of fast photoelectrons is adequate to account for the heating at higher altitudes. The heating at night is consistent with a corpuscular flux of soft electrons with a total energy of about 1×10^{-2} ergs cm^{-2} sec^{-2}.

i

CONTENTS

LIST OF ILLUSTRATIONS

LIST OF TABLES

DETAILED BEHAVIOR OF THE MIDLATITUDE IONOSPHERE

FROM THE EXPLORER XVII SATELLITE

INTRODUCTION

Between 1959 and 1961 a series of measurements of electron temperature using rocket-borne electrostatic probes at Ft. Churchill, Manitoba and at Wallops Island, Virginia, established that there are marked differences between the electron temperature and the heavy particle temperature in both daytime and nighttime ionospheres (Boggess, Brace and Spencer, 1959),[1] (Spencer, Brace and Carignan, 1962),[2] (Brace, Spencer and Carignan, 1963).[3] The data show also that the magnitude of the temperature difference increases with latitude, a conclusion in harmony with later observations from the Ariel satellite (Willmore, Henderson, Bowen and Boyd, 1964).[4]

It was clear that further measurements were desirable to determine more precisely the extent of non-equilibrium for a wide variety of ionospheric conditions, especially since the degree of thermal non-equilibrium is a sensitive indicator of atmospheric energy sources. Theoretical studies (Hanson and Johnson, 1961),[5] (Dalgarno, McElroy and Moffett, 1963),[6] (Hanson, 1963),[7] (Dalgarno, 1963)[8] had demonstrated the close relationship of the charged particle temperature and densities to the composition and structure of the neutral particle atmosphere, and thus had emphasized the need for simultaneous measurements of ionospheric and neutral particle parameters. Accordingly, cylindrical electrostatic probe experiments, similar to that employed in the rocket flights, were included with the neutral particle mass spectrometer and total density gauge experiments in the Explorer XVII satellite, (Reber, Nicolet, 1965)[9] (Newton, Horowitz, Priester, 1965).[10] A brief description of some of the satellite probe measurements has been given (Brace and Spencer, 1964).[11] In this paper, we shall report the probe results in more detail and discuss their significance in the context of the heat balance in the ionosphere.

THE ELECTROSTATIC PROBE EXPERIMENTS

The cylindrical probes employed for the measurements of electron temperature T_e and ion density N_i were dimensioned to operate in an orbital-motion-limited mode (Mott-Smith and Langmuir, 1926).[12] Each collector was 23 cm in

length and 0.056 cm in diameter. A guard electrode, 10 cm in length, was employed to prevent the collection of charged particles within the ion sheath surrounding the satellite. Both the collector and guard were made of stainless steel. The location of the sensors is discussed in an accompanying paper (Spencer, 1965).[13]

Figure 1 is a functional block diagram which applies for either the T_e or the N_i experiment. The electronic circuitry associated with each sensor provided suitable sawtooth sweep voltages and current measuring sensitivities to optimize one experiment for the determination of N_i and the other for the measurement of T_e. The experiments operated simultaneously throughout each 4-minute satellite pass and provided simultaneous point by point measurements of both T_e and N_i along the satellite path.
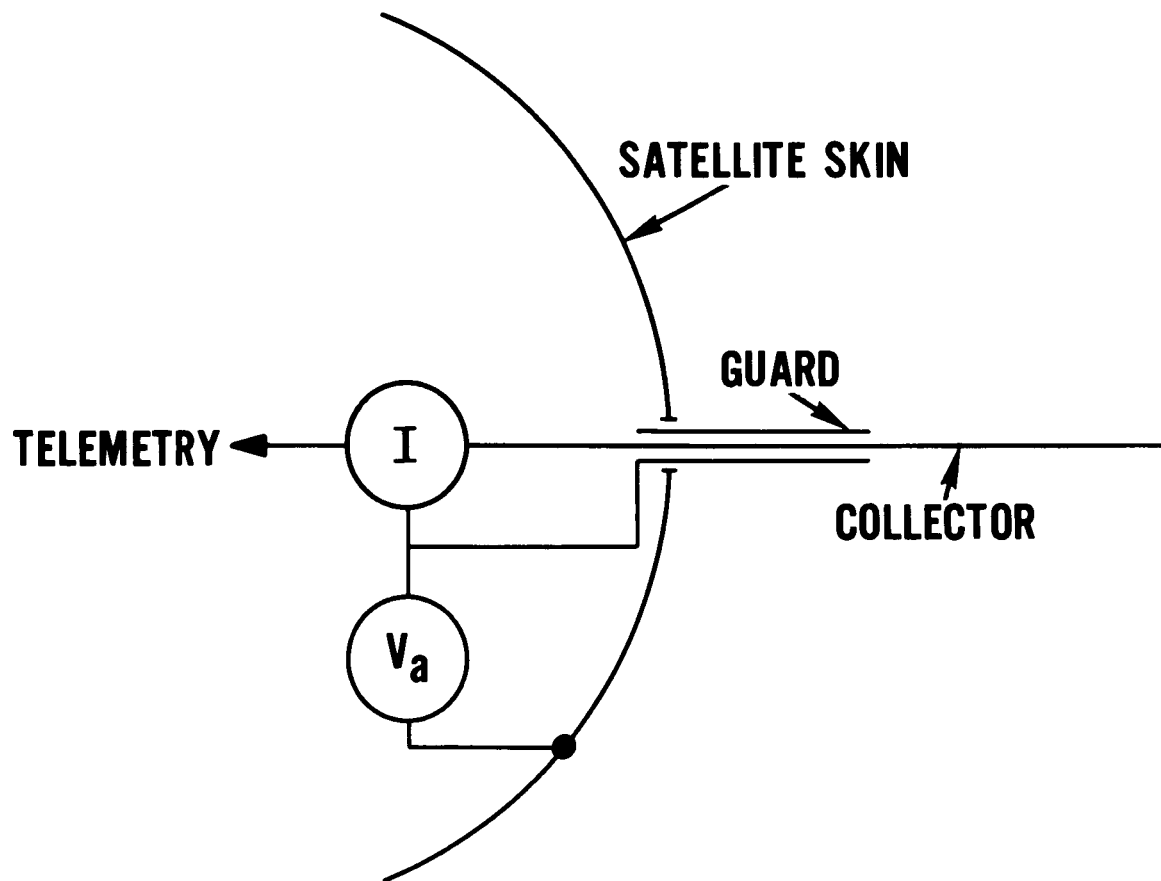
Figure 1—Functional Diagram of Either the Electron Temperature (T_e) or the Positive Ion Density (N_i) Probe Experiment

The Ion Density Measurement

The voltage applied between the N_i probe and the satellite was swept both negative and positive (-3 v to +2 v) so that both the ion and electron saturation regions of the volt-ampere characteristics were observed. Since the satellite potential was normally about -0.5 v, the probe potential V relative to the plasma was -3.5 to +1.5 v. The ion saturation region of a cylindrical collector (when employed on a satellite) is particularly useful for determining the local charged particle density because the flux of ions intercepted by the probe is determined largely by the satellite velocity and the collector orientation, which are known factors. Because of the high satellite velocity the ion current I_i is relatively insensitive to the thermal velocity of the ions and the accelerating potential of the collector, factors which are less well known.

Figure 2 shows a machine-plot of raw telemetry data points representing two consecutive volt-ampere characteristics from the N_i probe. At positive applied voltages the measured current is off-scale negative due to the predominance of electron current, and only the ion saturation regions are visible. The
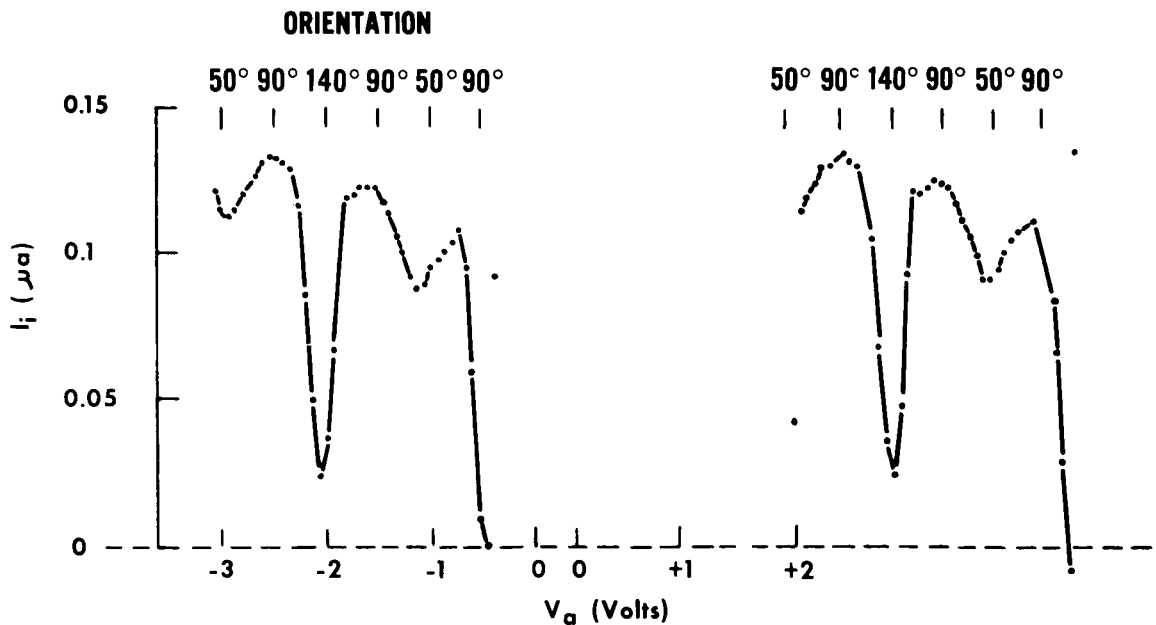
ORIENTATION

Figure 2—Raw Telemetry Data (Points) for Two Consecutive Volt-Ampere Characteristics of N_i Probe. The Ion Saturation Regions, Modulated by the Changing Probe Orientation, Display Maximum Ion Current when the Probe is Perpendicular to Velocity Vector (90°) and Minimum Current when the Probe Looks Forward (50° in this Case) and Aft (140°).

3

sweep period (2 seconds) was made several times the spin period (0.7 seconds) so that the effects of changes in orientation upon collection area and wake effects could be studied through the manner in which they modulate the ion saturation current. Maxima in the ion current (I_{max}) occur twice per satellite spin, corresponding to those times when the probe axis is perpendicular to the velocity vector. At this orientation the collector presents its maximum projected area to the plasma stream. In addition, a major minimum of ion current is observed each time the probe is rotated into the wake region behind the satellite. A secondary minimum occurs 180° later when the sensor is ahead of the satellite and presents its minimum projected area to the stream.

The relatively small effect of the applied voltage is evident in the slight decrease of I_{max} between successive maxima. This decrease corresponds to a voltage change of about 1 v. Curves such as those shown in Figure 2 permit one to derive empirically the functional dependence of I_{max} upon V, a relationship which is needed for an accurate evaluation of N_i from the measured ion currents. Using the slope of I_{max} versus V derived from a representative selection of probe data, I_{max} was found to be about 20% ± 3% higher than would be observed at V = 0, where no acceleration of the ions occurs. Neglecting a very small enhancement of the current due to the thermal motion of the ions (<4%), the current at V = 0 is simply the charge per unit time swept out by the frontal area of the collector. Therefore the ambient positive ion density is given by:

$$N_i = \frac{0.8\ I_{max}}{1\ d\ e\ v_s} = V = 0 \tag{1}$$

where 1 is the length and d is the diameter of the collector, e is the unit charge and v_s is the satellite velocity.

Because I_i is always measured at the same orientation, the relative accuracy of the N_i measurements depends primarily upon the current detection error, which does not exceed 5% for $N_i > 5 \times 10^4$ cm^{-3}. The absolute accuracy of N_i is better than 10% when 0^+ ions predominate (below 600 km).

The Electron Temperature Measurement

Between the extremes of ion and electron saturation, the probe current characteristic exhibits an exponential shape whose curvature permits a direct interpretation of the curves in terms of the electron temperature (Mott-Smith and Langmuir, 1926).[12] The analysis of individual curves is carried out by the log-plot technique in which T_e is given by the slope of $\log_e I_e$ with respect to V,

4

as given by (2)

$$\frac{d \log_e I_e}{dV} = - \frac{e}{kT_e} \qquad (2)$$

Based on the experience gained with identical probes on ejectable rocket-borne instruments (Spencer, Brace and Carignan, 1962),[2] the T_e experiment was designed to permit high resolution of the exponential portion of the volt-ampere characteristics, with primary emphasis on thermal electrons in the 0 - 1 eV range. To permit ample voltage resolution through a wide range of T_e, two saw-tooth sweeps were employed (0 to +0.75 v and 0 to +1.5 v). The telemetry sampling rate assigned to the experiment (180 samples/sec) was sufficient to permit a sweep rate of 10 curves per second. The necessary current resolution was provided by two linear current detectors of 1 μa and 5 μa full scale sensitivity which time-shared the assigned telemetry channels on a 10-second-on, 10-second-off basis. Each detector recorded 100 consecutive volt-ampere curves during its on-period.

Figure 3 is a computer plot of 1 μa and 5 μa raw telemetry data at the beginning of two consecutive 10 second on-times recorded during a nighttime Blossom Point pass. The temperature and density at this time were moderately low

T_e Probe Volt-ampere Characteristics
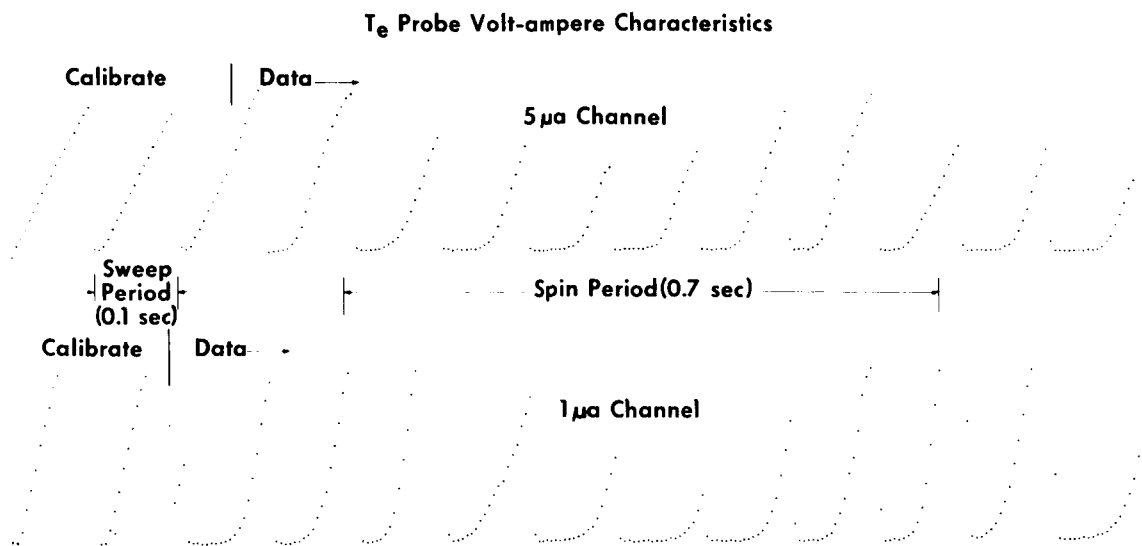
Figure 3–Raw Telemetry Data Showing a Series of 5 μa (0 to 1.5 v Applied) and 1 μa (0 to 0.75 v) Current Characteristics, Each Preceded by an Inflight Current Calibration. The 1 μa Channel Provides the High Resolution Necessary to Permit Accurate Determination of the Low Electron Temperature in Nighttime Passes Such as this One.

$(T_e \simeq 1200°K,\ N_i \simeq 1 \times 10^5\ cm^{-3})$. The inflight current calibrations at the left were obtained by substituting appropriate known resistances for the probe sensor at the beginning of each 10 second series of curves. The 5 μa data taken with a 1.5 v sweep permit a "coarse" measurement of the characteristics. A "high resolution" measurement is provided by the 1 μa detector with a 0.75 volt sawtooth applied. This combination of sensitivities and voltages permitted high resolution measurements of T_e between 500° and 5000°K, when N_i exceeded $3 \times 10^4\ cm^{-3}$. The satellite spin period is apparent in Figure 3 in the modulation envelope of the electron current curves (not particularly marked in this example). This modulation stems from both the reduction of charged particle density in the wake region immediately behind the satellite and the modulation of probe voltage by the induced $\bar{B} \times \bar{v}_s$ voltage caused by motion of the satellite through the Earth's magnetic field, $\bar{B}$. Measurement error due to these easily recognized effects has been avoided by selecting for analysis only those non-wake curves which correspond to the minimum rate of change of induced voltage. Following this criterion for curve selection, the relative accuracy of the T_e measurements within a given satellite pass is better than 5%. The absolute accuracy depends upon the maintenance of the linearity and amplitude of the sawtooth sweep voltage throughout the life of the satellite. Frequent checking of inflight calibrations has shown no detectable change and the absolute accuracy is believed to be better than 5% on most passes.

Figure 4a and 4b help to demonstrate the computer methods employed in the T_e analysis. Figure 4a is a computer printout arranged to display a single volt-ampere characteristic as it appeared on the 1 μa channel, and 4b is a log-plot of the same characteristic. Because of a limited plotting interval imposed by the printer, the plotting accuracy shown is only 1/10th the accuracy of the actual data. The computer is programmed to make a best straight-line fit to the linear part of the log plot and then print out the corresponding T_e according to equation (2). Plots of this type are made by the computer for each curve of a group of 15 consecutive curves. Several groups are chosen from each satellite pass to permit hand verification of the computer values of T_e. All temperature data presented in this paper have been verified in this manner.

RESULTS

Motion of the Satellite

The inclination of a satellite orbit simultaneously determines the precession rate of the orbit plane and the movement of perigee, so that a given satellite may sample the atmosphere at only unique combinations of local times and altitudes over each telemetry station. Thus, the orbital inclination determines the
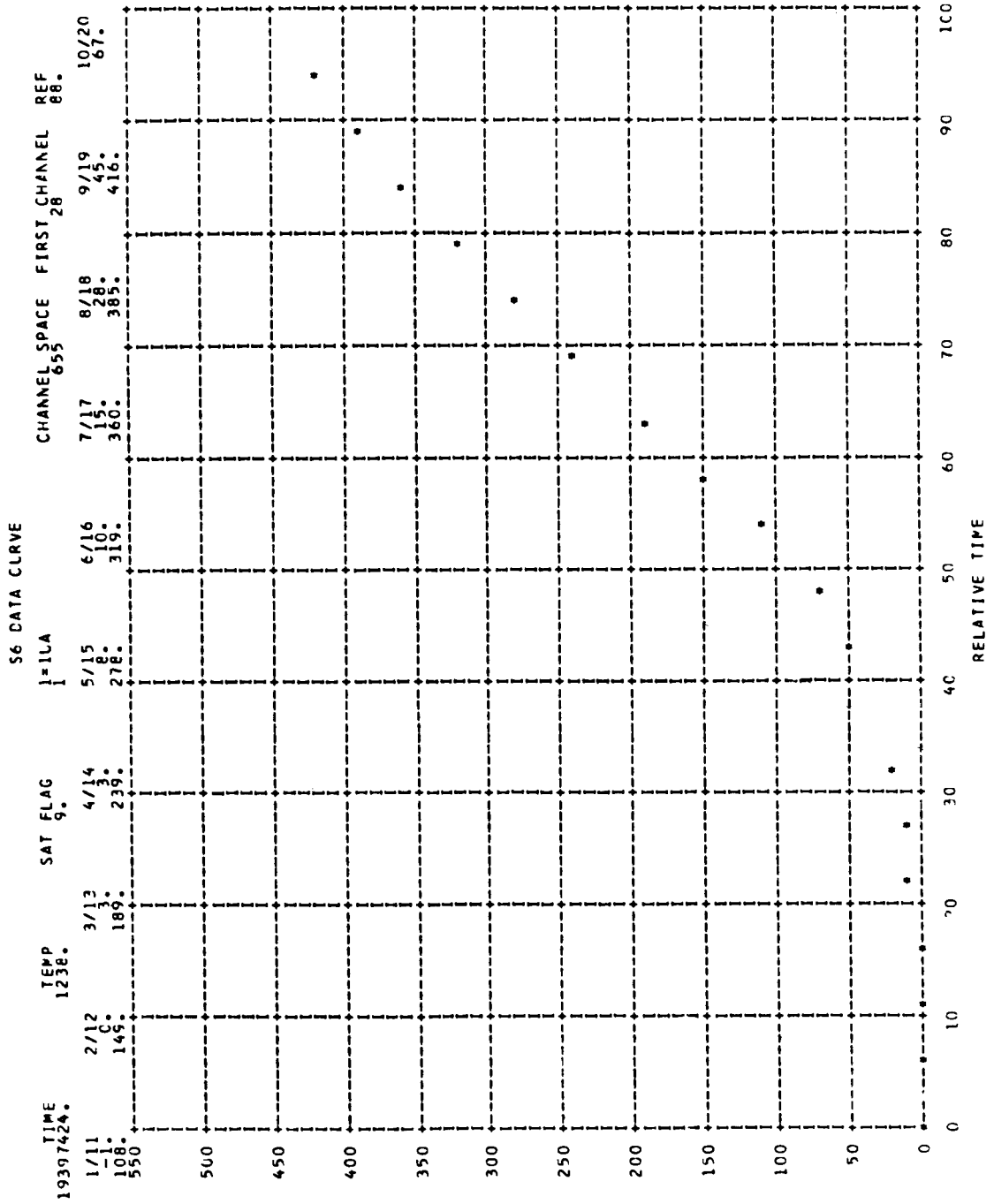
Figure 4a–Computer Plot of Single Current Characteristic Demonstrating the Computer Analysis Procedure. Telemetered Points (Current) are Plotted Versus Time (Voltage, 0→0.75 v) to Permit Visual Identification of Exponential Portion of Curve (0 ⊢ 60 Milliseconds).
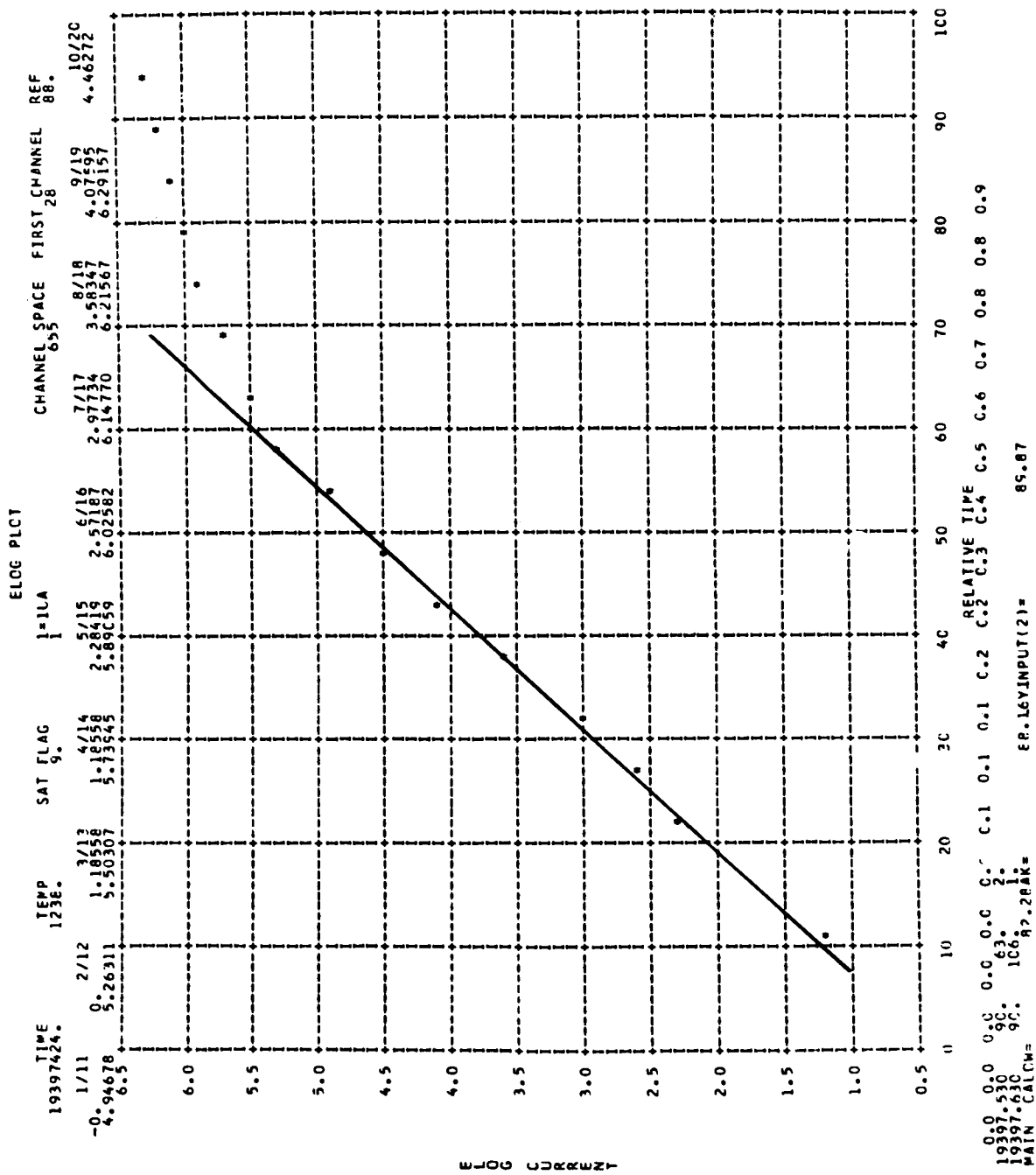
Figure 4b—Computer Plot of Natural Log of Currents in Figure 4a showing the Linear Portion which is Related to T_e. Line Drawn by Hand Permits Manual Check of Computer Value of T_e Printed Automatically above.

8

aeronomic coverage which a particular satellite can provide. For example, in its 100 day lifetime, Explorer XVII's inclination of 58°, combined with apogee and perigee altitudes of 927 and 258 km, provided the coverage over Blossom Point shown in Figure 5. Each pair of points connected by a line represents the beginning and end of a particular satellite pass. Although the pattern of coverage was similar at other latitudes, perigee and apogee occurred at other local times.

Figure 5 aids in selecting those Blossom Point passes in which diurnal and altitude effects can be most effectively separated. For example, the southbound set of passes provides an excellent opportunity to study the diurnal variation of T_e and N_i at a fixed altitude (perigee) through the daylight hours.

In processing the data from each telemetry station we derived a single value of T_e and of N_i from groups of volt-ampere curves taken at one-minute intervals through each satellite pass and plotted the beginning-of-pass and end-of-pass values of T_e and N_i against local solar time. Although the gross variations evident in the resulting local time plots for each station may reflect some altitude and seasonal variations in the atmosphere, the rapid precession of the orbit plane ensures that local time effects will predominate. Variations of T_e and N_i within a particular pass, however, are controlled by latitude or altitude changes in that pass because the local time change within a pass is small.

Blossom Point Data

Table 1 contains the values of T_e and N_i measured at the beginning and end of each Blossom Point pass, with the corresponding positions of the satellite and concurrent values of the solar index ($F_{10.7}$) and of the magnetic index (a_p).

To permit the local time, altitude, latitude and season of each measurement to be identified, data from southbound and northbound passes have been plotted separately in Figures 6 and 7, respectively. The points joined by lines are the beginning and end-of-pass values and the figures show the average altitude and the month of the pass.

Latitude and Local Time Effects – In order to show the effects of latitude, smoothed curves have been drawn in Figure 6 through the values measured at magnetic latitudes of 40°N and 55°N, the extremes of latitude observed from Blossom Point. The smoothed curves therefore represent an averaged diurnal variation of T_e and N_i near F_2 maximum at the indicated magnetic latitudes. The major characteristics of the diurnal variation of electron temperature are a nighttime minimum, a steep rise to a mid-morning maximum, and an afternoon
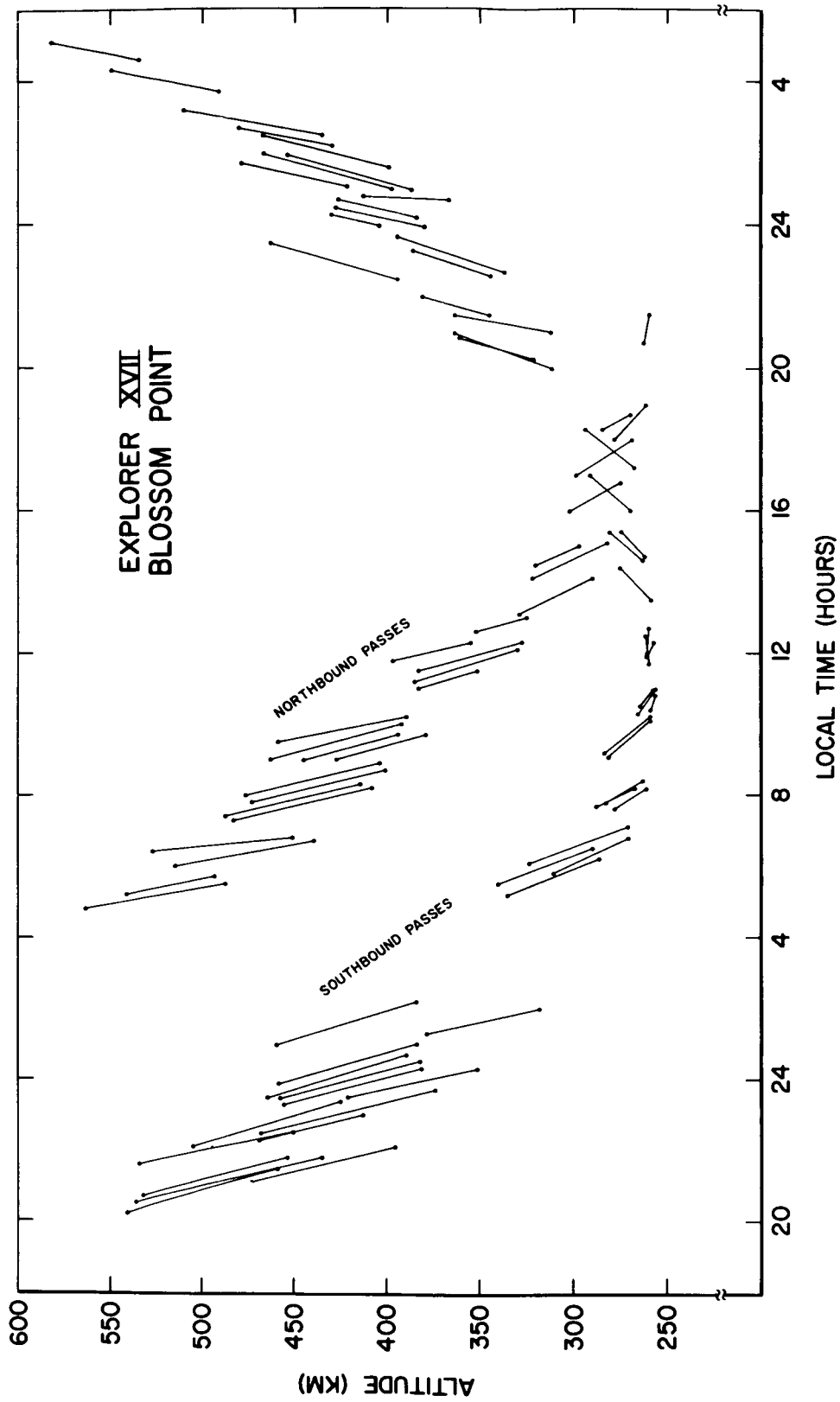
Figure 5—Altitude and Local Solar Time Coverage over Blossom Point Produced by the Precession of the Orbit Plane and the Movement of Perigee During the 100-Day Active Lifetime of Explorer XVII. The Points Joined by Lines Represent the Positions of the Satellite at the Beginning and End of Each Pass.

TABULATION OF T_e AND N_i FROM BLOSSOM POINT PASSES (EXPLORER XVII)

PASS	DATE	GMT (hr:min)	GEOGRAPHIC LATITUDE (degrees)		GEOGRAPHIC LONGITUDE (degrees)		ALTITUDE (kilometers)		LOCAL TIME (hours)		T_e (degrees Kelvin)		N_i (part./cc)		$F_{10.7}$	a_p
			begin	end	begin	end	begin	end	begin	end	begin	end	begin	end		
15	4/4/63	2:10	33	43	-82	-70	263	260	20.7	21.5	1100	1150	2.6 +5	2.4 +5	70	3
50	4/6/63	10:47	35	27	-93	-86	534	592	4.6	5.1	1650	1650	5.5 +4	7.8 +4	78	22
79	4/8/63	9:20	39	30	-84	-77	492	550	3.7	4.3	1350	1125	2.2 +4	7.2 +4	81	9
118	4/10/63	23:35	30	36	-80	-68	285	270	18.3	18.7	1600		1.0 +6		82	2
123	4/11/63	7:59	41	32	-82	-73	446	510	2.5	3.2	1525	1625	6.4 +4	6.8 +4	88	3
138	4/12/63	8:40	41	35	-88	-82	440	481	2.2	2.7	1700	1700	6.5 +4	6.7 +4	93	7
148	4/12/63	23:47	35	46	-86	-73	279	262	18.0	19.0	1800	1800	7.7 +5	6.7 +5	73	7
152	4/13/63	6:32	46	36	-77	-64	400	468	1.6	2.5	1300		6.9 +4		89	4
167	4/14/63	6:35	46	36	-84	-70	388	456	1.0	2.0	1500		4.5 +4		87	4
182	4/15/63	6:43	43	33	-87	-74	398	467	1.0	2.0	1300		3.9 +4		88	27
192	4/15/63	22:25	32	43	-85	-72	299	269	17.0	18.0	2600		3.6 +5		88	5
197	4/16/63	6:49	38	30	-85	-78	427	479	1.2	1.7	1700	1700	4.4 +4	5.4 +4	88	4
211	4/17/63	5:15	46	39	-78	-68	368	414	0.1	0.8	1250	1200	6.3 +4	9.2 +4	87	7
226	4/18/63	5:21	43	36	-79	-71	385	427	0.2	0.7	1400	1250	7.7 +4	7.6 +4	88	3
236	4/18/63	21:04	34	44	-78	-68	303	275	16.0	16.8	1850	1700	7.5 +5	8.2 +5	88	27
241	4/19/63	5:25	42	34	-84	-75	381	429	23.9	0.5	1550	1425	5.4 +4	9.0 +4	84	18
256	4/20/63	5:34	37	33	-84	-80	405	431	24.0	0.3	1750	1250	6.7 +4	9.0 +4	78	6
270	4/21/63	3:55	47	37	-81	-66	338	396	22.7	23.7	1250		6.7 +4		74	3
285	4/22/63	4:40	45	38	-82	-73	345	387	22.6	23.3	1300	1300	2.4 +5	1.5 +5	72	3
310	4/23/63	19:51	36	42	-81	-75	321	298	14.5	15.0	2300	2000	2.4 +5	2.4 +5	71	3
325	4/24/63	19:57	37	47	-86	-72	322	282	14.2	15.2	2050		3.2 +5		73	4
330	4/25/63	4:21	32	22	-89	-79	396	464	22.5	23.5	1650		6.7 +4		72	6
359	4/27/63	2:52	39	32	-82	-70	346	382	21.5	22.0	1700		1.2 +5		75	6
384	4/28/63	18:39	40	49	-82	-69	329	290	13.2	14.2	2000		3.0 +5		78	4
388	4/29/63	1:32	44	32	-75	-61	313	365	21.0	21.4	1500	1650	1.9 +5	1.1 +5	78	3
398	4/29/63	17:04	36	41	-68	-62	353	325	12.6	13.0	2250		2.5 +5	2.8 +5	78	4
413	4/30/63	17:07	29	36	-83	-73	398	356	11.8	12.3	2800	3200	2.9 +5	2.9 +5	80	39
418	5/1/63	1:32	39	31	-80	-72	323	362	20.3	20.8	2080	2100	4.4 +5	2.4 +5	82	80
443	5/2/63	17:18	34	44	-88	-76	384	328	11.5	12.3	2500		2.1 +5		82	32
458	5/3/63	17:22	35	45	-95	-81	386	330	11.2	12.1	2200	2400	2.4 +5	2.2 +5	81	18
472	5/4/63	15:49	36	42	-73	-67	384	352	11.0	11.5	2250	2500	2.1 +5	2.6 +5	82	18
506	5/6/63	22:41	49	39	-83	-67	268	294	17.2	18.3	2500	2300	4.1 +5	4.8 +5	87	6
516	5/7/63	14:23	27	39	-75	-64	460	390	9.5	10.2	2900	2750	2.2 +5	2.2 +5	88	6
531	5/8/63	14:27	28	39	-80	-69	464	393	9.0	10.0	3000	3000			86	7
546	5/9/63	15:32	32	40	-82	-73	446	395	9.0	9.7	3000	3000	1.7 +5	1.8 +5	88	9
561	5/10/63	14:37	36	44	-85	-70	428	380	9.0	9.7	2800	2800	1.9 +5	1.8 +5	87	9
590	5/12/63	13:06	31	42	-77	-65	477	405	8.0	8.9	2700		1.2 +5		87	9
595	5/12/63	21:28	42	32	-83	-70	270	292	16.0	17.0	2450	2100	5.4 +5	7.6 +5	87	7
605	5/13/63	13:08	33	43	-81	-68	474	402	7.8	8.7	2400	2450	1.7 +5	1.7 +5	89	23

TABULATION OF T_e AND N_i FROM BLOSSOM POINT PASSES (EXPLORER XVII)

PASS	DATE	GMT (hr:min)	GEOGRAPHIC LATITUDE (degrees) begin	end	GEOGRAPHIC LONGITUDE (degrees) begin	end	ALTITUDE (kilometers) begin	end	LOCAL TIME (hours) begin	end	T_e (degrees Kelvin) begin	end	N_i (part./cc) begin	end	$F_{10.7}$	a_p
620	5/14/63	13:13	32	43	-88	-75	488	415	7.4	8.3	2600	2600	1.3 +5	1.3 +5	95	6
635	5/15/63	13:17	34	45	-91	-78	482	409	7.3	8.2	2600	2600	1.5 +5	1.6 +5	98	5
654	5/16/63	20:06	43	34	-82	-69	262	275	14.7	15.4	2400	2400	5.6 +5	6.7 +5	100	2
669	5/17/63	20:10	40	30	-84	-72	263	281	14.6	15.4	2200	2000	5.9 +5	7.6 +5	100	12
679	5/18/63	11:49	36	41	-87	-75	527	452	6.4	6.8	2100	2100	1.2 +5	1.2 +5	98	3
694	5/19/63	11:53	36	44	-88	-79	515	440	6.0	6.7	2500	2450	1.2 +5	1.3 +5	99	3
698	5/19/63	18:58	44	36	-76	-66	259	265	13.5	14.4	2450	2100	4.7 +5	6.4 +5	99	6
723	5/21/63	10:21	33	39	-78	-71	542	494	5.2	5.7	2700	2700	5.7 +4	6.6 +4	88	2
738	5/22/63	10:24	31	41	-85	-74	562	488	4.8	5.5	2500		6.3 +4		89	2
772	5/24/63	17:15	44	41	-80	-76	261	258	12.0	12.3	2000	2000	4.8 +5	5.1 +5	89	3
787	5/25/63	17:19	41	32	-82	-73	261	260	11.8	12.7	2400	2050	4.7 +5	7.4 +5	83	7
802	5/26/63	17:22	41	29	-84	-76	260	262	11.7	12.5	2600		3.9 +5		76	4
846	5/29/63	15:52	43	37	-81	-74	265	258	10.5	11.0	2600	2750	3.8 +5	3.4 +5	80	4
861	5/30/63	15:55	42	33	-86	-76	266	257	10.3	11.0	3000	3000			83	5
876	5/31/63	15:58	37	30	-85	-79	259	257	10.4	10.8	2950	2700	4.5 +5	4.9 +5	89	6
890	6/1/63	14:22	47	36	-80	-65	282	259	9.1	10.1	3150		3.0 +5		84	11
905	6/2/63	14:24	46	34	-86	-71	284	259	9.2	10.2	2750			3.2 +5	81	15
964	6/6/63	12:57	43	36	-77	-68	288	268	7.7	8.2	2200	2200	2.8 +5	5.1 +5	77	5
979	6/7/63	12:59	41	32	-79	-70	282	263	7.8	8.4	2750	2850	3.5 +5	4.6 +5	84	22
994	6/8/63	13:02	38	29	-80	-74	278	261	7.6	8.2	3000	2800	2.8 +5	4.7 +5	90	6
1023	6/10/63	11:27	48	34	-78	-63	324	271	6.1	7.1	2500	2000	2.2 +5	4.7 +5	99	5
1038	6/11/63	11:27	50	40	-90	-74	341	290	5.5	6.5	2000	2000	2.8 +5	2.4 +5	103	4
1053	6/12/63	11:31	43	31	-84	-71	311	271	5.8	6.8	2200	1950	2.9 +5	4.4 +5	109	6
1068	6/13/63	11:31	47	36	-95	-81	336	287	5.2	6.2	2200	1900		4.0 +5	107	6
1260	6/26/63	6:57	52	42	-100	-83	460	385	1.0	2.2	1100	1100	5.4 +4	9.0 +4	74	48
1275	6/27/63	7:02	40	28	-86	-75	379	318	1.3	2.0	1375	1150	1.1 +5	1.2 +5	72	18
1289	6/28/63	5:24	50	40	-83	-67	459	384	23.9	1.0	1250	1175	3.2 +4	1.1 +5	74	6
1304	6/29/63	5:25	50	40	-88	-72	465	389	23.5	0.7	1700	1425	4.6 +4	6.9 +4	73	4
1319	6/30/63	5:26	48	37	-89	-74	458	382	23.5	0.5	1250	1100	4.5 +5	7.7 +4	76	12
1334	7/1/63	5:28	47	36	-92	-78	456	381	23.3	0.3	1375	1325	5.5 +4	1.4 +5	76	7
1349	7/2/63	5:31	41	29	-89	-77	421	351	23.5	0.3	1200	1050	6.3 +4	1.2 +5	77	3
1363	7/3/63	3:52	50	41	-86	-69	505	425	22.1	23.4	1750	1400	9.5 +4	1.1 +5	78	2
1378	7/4/63	3:54	45	31	-81	-65	468	374	22.5	23.7	1250	1250	9.9 +4	3.0 +5	78	5
1393	7/5/63	3:55	47	37	-89	-75	492	413	22.0	23.0	1700	1550	8.6 +4	9.9 +4	78	32
1408	7/6/63	3:57	50	41	-101	-82	534	451	21.6	22.5	1125	1125	9.0 +4	1.8 +5	77	67
1423	7/7/63	3:58	43	31	-93	-80	473	396	21.1	22.1	1100	1100	8.1 +4	2.2 +5	77	9
1437	7/8/63	2:20	49	39	-85	-69	531	454	20.7	21.8	1650	1650	1.4 +5	1.2 +5	77	15
1452	7/9/63	2:21	49	34	-88	-70	538	435	20.5	21.8	2250	1500	2.1 +5	3.0 +5	77	27
1467	7/10/63	2:22	48	35	-92	-74	541	459	20.2	21.5	2150	1850	1.4 +5	1.4 +5	76	6
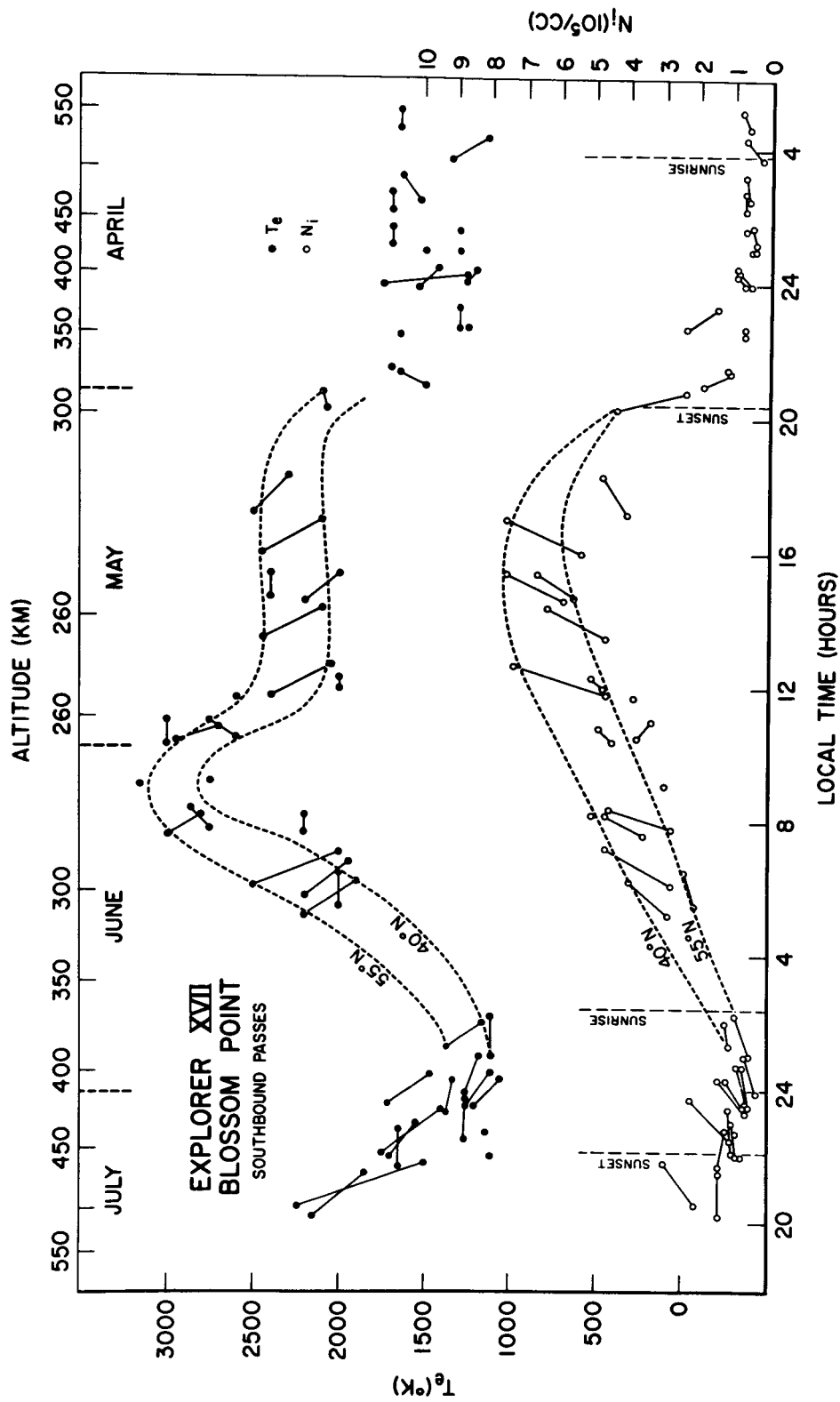
Figure 6—T_e and N_i data from Southbound Blossom Point Passes Identified with the Altitude, Month, and Local Times. The Points Joined by Lines Represent Beginning-Of-Pass and End-Of-Pass Values. The Latitude Gradient in T_e and N_i, Evident in the Daytime, Made Possible Latitude Identification of the Data as Well.
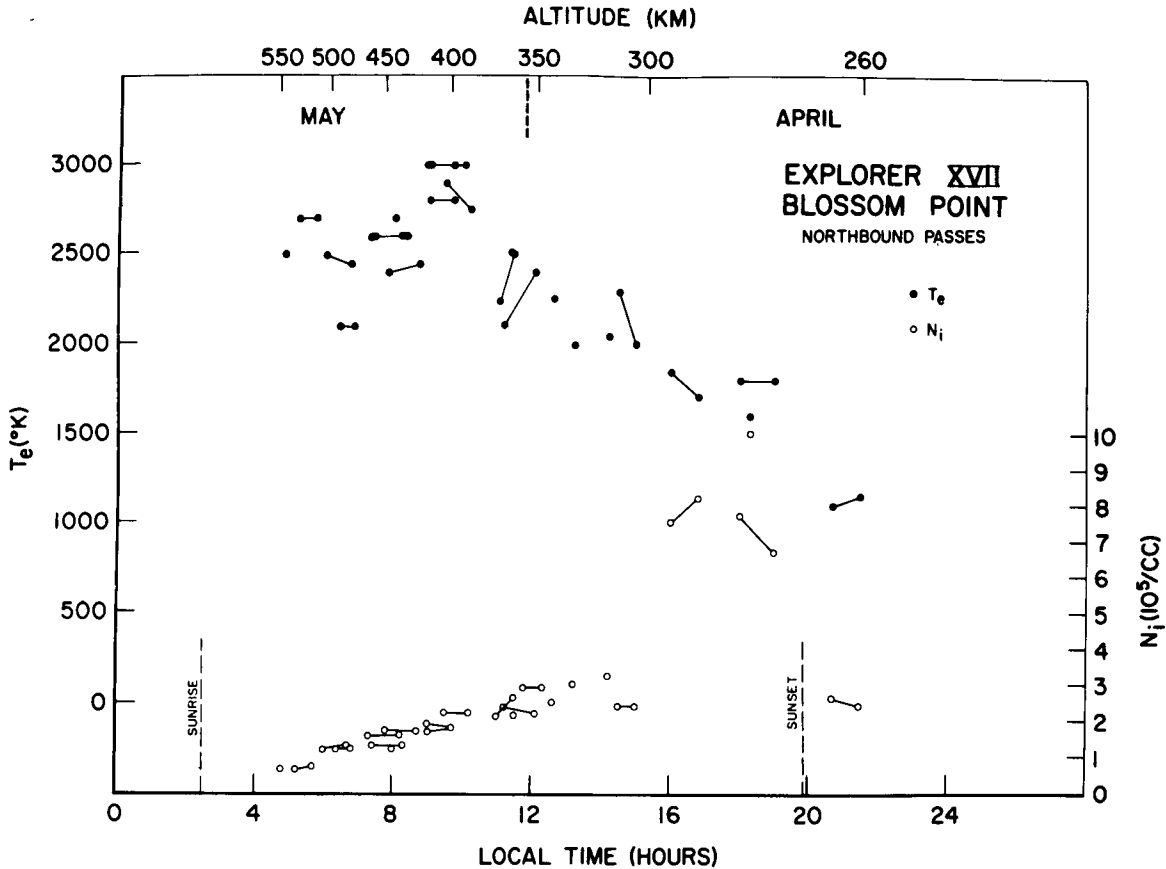
Figure 7—T_e and N_i Data from Southbound Blossom Point Passes.

plateau, followed by a decline to a lower, more variable, value at night. This behavior is very different from the diurnal variation of the neutral gas temperature (T_g), which exhibits a maximum in the afternoon rather than the morning. The values of T_e are clearly much in excess of T_g, even at night. The diurnal variation in N_i is characterized by a gradual morning rise, an afternoon maximum and a sharp decrease at sunset.

It is particularly significant that in all southbound daytime passes the satellite was near perigee and therefore was changing altitude very little. Thus the changes in T_e and N_i observed within each of these passes must reflect the latitude control which was first evident in the smoothed diurnal variation curves for 40° and 55° N magnetic latitude. The average temperature gradient is about 25°K/° latitude, at this latitude and altitude.

14

Seasonal Effects — A major seasonal effect which may be seen in Figure 6 is made evident by the longer time T_e remained low in the April night passes as compared to the June-July night passes when nights were shorter. The less rapid decay of T_e at sunset in July than at sunset in April may also be a seasonal effect, or it may simply reflect the greater influence of heat conduction in the electron gas at the higher altitude of the July sunset passes.

Altitude Effects — The night-time passes in April (Figure 6), where altitude is the most important variable, suggest that there is a slight positive gradient of T_e with altitude at night of the order of $1°K/km$ between 350 and 550 km.

As noted earlier, a comparison of northbound passes (Figure 7) and southbound passes (Figure 6) permits the effect of altitude to be evaluated for the morning hours. Such a comparison reveals no systematic gradient of T_e with altitude between 0600 and 1200 hours.

Inverse Relationship Between T_e and N_i — In nearly all daytime passes where beginning and end values of T_e and N_i have been derived, T_e increased and N_i decreased with increasing latitude, the changes being especially marked in the southbound passes which were at lower altitudes. A few exceptions occurred in the early morning, higher altitude, passes when neither T_e nor N_i changed significantly within individual passes.

Data from Other Latitudes

Graphs of the measurements of T_e and N_i during passes at Quito, Equador ($10°N$ magnetic) and at College, Alaska ($60°N$ magnetic) have been prepared. The smoothed diurnal variations of T_e and N_i derived from all three stations are shown in Figure 8. These curves refer to the region between 260 and 400 km containing the F_2 maximum. Although the general behavior of the F-region at Blossom Point, Quito and College is similar, the times of the morning maxima of T_e and afternoon maxima of N_i and the magnitudes of the temperatures and densities differ considerably. Not all the differences can be ascribed to magnetic latitude alone, for the T_e maximum at College may occur earlier because of the earlier sunrise there in summer, which is a result of the higher geographical latitude. Indeed, the Blossom Point results at $40°$ and $55°N$ magnetic latitude suggest that magnetic latitude has little control over the time of occurrence of the maxima in T_e. Differences in magnetic longitude may also be of importance.

The higher nocturnal electron temperatures of the College passes also may be related to the higher geographic latitude ($58°N$) at which they were measured.
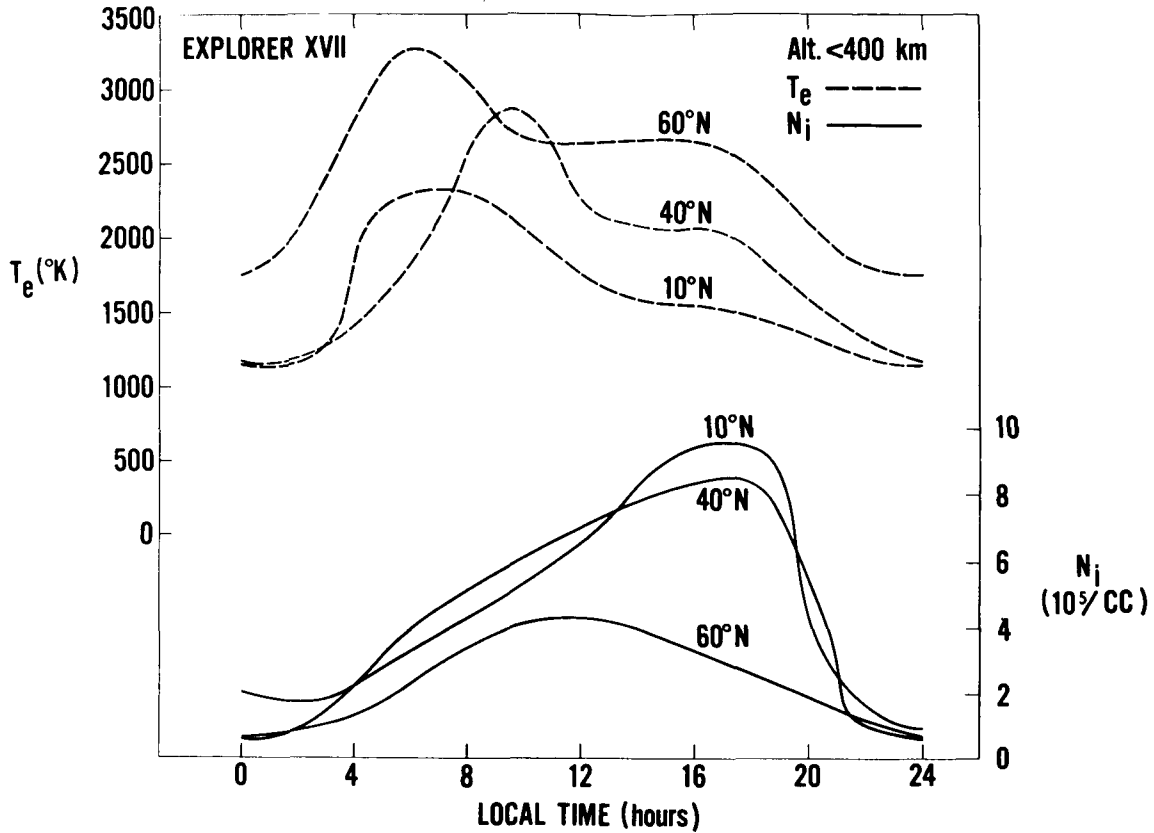
Figure 8–Smoothed Diurnal Variations in T_e and N_i at Three Latitudes (10°, 40°, and 60° North Magnetic) for Altitudes Below 400 Kilometers.

The mid-summer F_2 region at 58°N is always illuminated, although the zenith angle of the sun exceeds 90° near midnight.

ION TEMPERATURE AND HEAT SOURCE

If we assume that the temperature of the electron gas is in equilibrium such that the rate at which it gains heat equals the rate at which it loses heat, the heat source Q necessary to maintain a temperature difference can be calculated from the cooling rates. Only elastic processes contribute significantly to cooling in collisions with the positive ions, and the rate at which the electron gas loses heat to a positive ion gas mixture of O^+, He^+ and H^+ at a temperature T_i is given approximately by

$$Q_e = \frac{5 \times 10^{-7} (T_e - T_i) n_e}{T_e^{3/2}} \left\{ n(O^+) + 4n(He^+) + 16n(H^+) \right\} \, eVcm^{-3} \, sec^{-1} \quad (3)$$

16

(cf. Spitzer 1956),[14] (Hanson and Johnson, 1961).[5] Equation (3) demonstrates that simultaneous measurements of temperature and density are required for an accurate calculation of the energy source responsible for the temperature difference. The strong inter-dependence of temperature and density require that the measurements be essentially point measurements.

The Positive Ion Temperature

The heat gained by the positive-ion gas causes its temperature to rise above that of the neutral particle gas (Hanson, 1963)[7] (Dalgarno, 1963).[8] The positive ions cool mainly by resonance charge transfer collisions with the parent atoms and by elastic collisions with unlike atoms and molecules. The rates of heat loss from the positive ions to the neutral gas at a temperature T_g may be derived from the collision frequencies (Dalgarno, 1958, [15] 1961,[16] 1964[17]) and there results

$$Q(O^+) = n(O^+) \left\{ 9 \times 10^{-14} \, n(0) + 6 \times 10^{-14} \, n(N_2) \right.$$
$$\left. + 6 \times 10^{-15} \, n(He) + 2 \times 10^{-15} \, n(H) \right\} \, (T_i - T_g) \, eV \, cm^{-3} \, sec^{-1}, \quad (4)$$

$$Q(He^+) = n(He^+) \left\{ 6 \times 10^{-14} \, n(0) + 4 \times 10^{-14} \, n(N_2) \right.$$
$$\left. + 2 \times 10^{-13} \, n(He) + 1 \times 10^{-14} \, n(H) \right\} \, (T_i - T_g) \, eV \, cm^{-3} \, sec^{-1} \quad (5)$$

and

$$Q(H^+) = n(H^+) \left\{ 3 \times 10^{-14} \, n(0) + 3 \times 10^{-14} \, n(N_2) \right.$$
$$\left. + 5 \times 10^{-14} \, n(He) + 4 \times 10^{-13} \, n(H) \right\} \, (T_i - T_g) \, eV \, cm^{-3} \, sec^{-1}. \quad (6)$$

In equilibrium,

$$Q_e = Q(O^+) + Q(He^+) + Q(H^+), \quad (7)$$

an equation which determines T_i in terms of T_e, n_e and the neutral particle and positive-ion concentrations.

17

The altitudes of the Blossom Point measurements were usually such that O^- was the major ion and thus (7) can be simplified to yield,

$$T_i - T_g = \frac{6 \times 10^6 \, n_e \, (T_e - T_i)}{n(0) \, T_e^{3/2}} .$$

(8)

We have substituted the satellite measurement of $N_i = n_e$ and of T_e into (8) together with the number densities of atomic oxygen given by the model of Harris and Priester (1962)[18] for the local time of the measurement. The resulting values of T_i and of T_e/T_i for Blossom Point are shown in Figures 9 and 10 as a function of altitude. In Figure 9 the passes divide naturally into those occurring in mid-morning (when T_e reaches its maximum), near sunset and at night. Figure 9 reveals a positive-ion temperature increasing with altitude, a difference between T_i and T_g first emerging in the region of 300 km. The positive-ion temperature is larger during the day than at night but even at night it appears to exceed T_g at high altitudes. Local time effects are distinguished in Figure 10 only between day and night but the data are probably sufficiently numerous to establish that during the day T_e/T_i passes through a maximum value of between 2 and 3 at an altitude near 300 km and approaches unity at high altitudes. Similar descriptions of the average T_e variations with altitude and of T_e/T_i have been given by Evans (1964)[19] and by Evans and Lowenthal, (1964)[20] in analyses of ground-based radar observations made at the latitude of the Blossom Point passes.

The Heat Source

Having determined T_i, the rate of heat loss of the heated electrons to the positive ion gas may be computed. The heated electrons also cool in collisons with the neutral particle gas, the most significant processes being excitation of atomic oxygen to the 'D level at high altitudes and rotational and vibrational excitation of molecular nitrogen at low altitudes. Cooling by excitation of oxygen to the 'D level is of special importance since it may be responsible for the variability in the intensity of the red arc in the dayglow (Noxon 1964),[21] (Dalgarno and Walker, 1964).[22] The cooling rates have been tabulated by Dalgarno and McElroy (1964)[23] and a comparison of the contributions of the various processes at an altitude of 250 km is given in Figure 11.

The accuracy of the cooling rates is not yet adequate to warrant the use of the neutral particle densities and temperatures measured by the other Explorer XVII experiments (Newton, et al, 1964),[10] (Reber, et al, 1964).[9] To calculate the heat necessary to produce the measured electron temperature we have instead
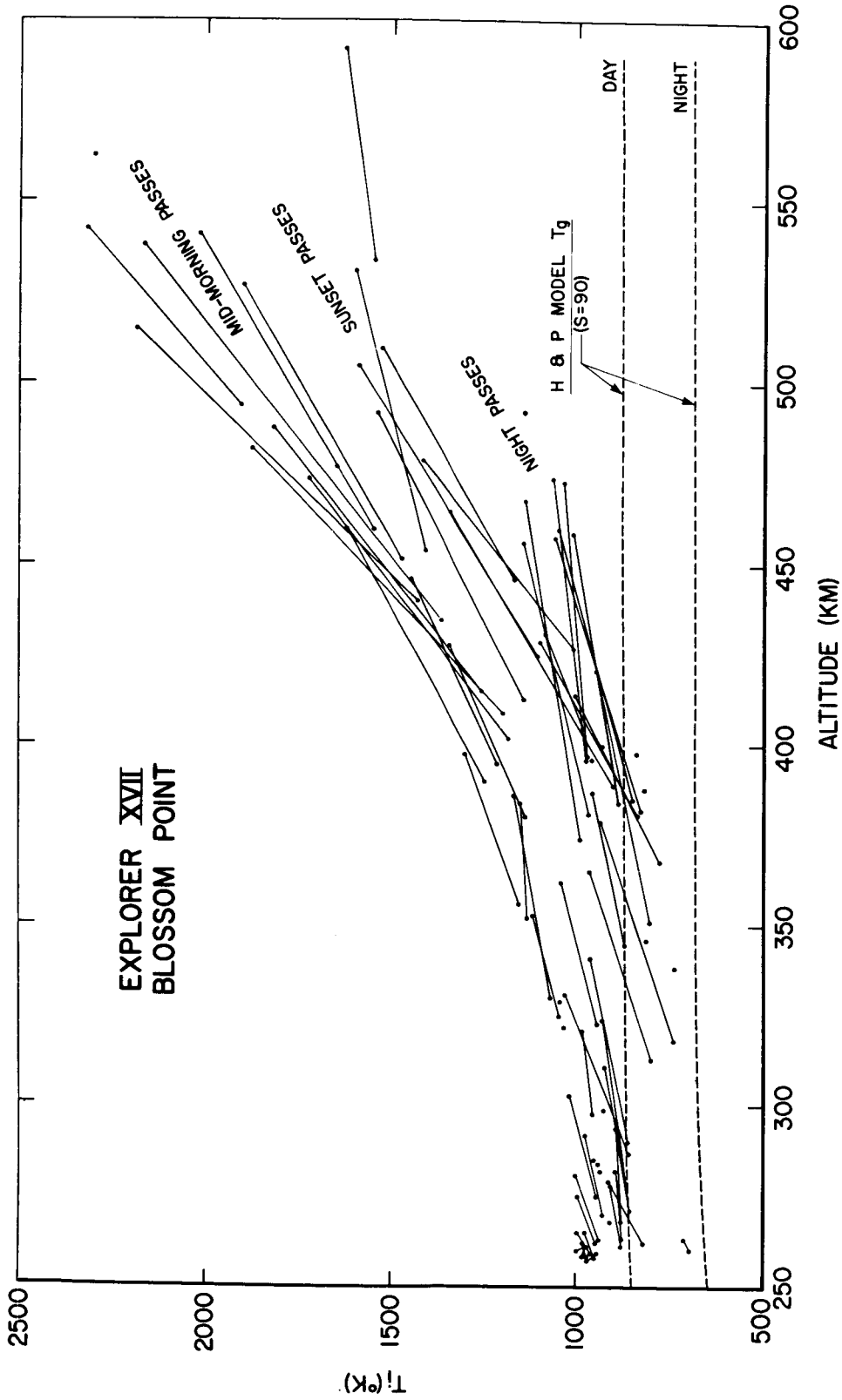
Figure 9–Calculated Ion Temperature (T_i) for All Blossom Point Passes. The Harris and Priester Models, used with Measured T_e and N_i for Computation, Are Also Shown.
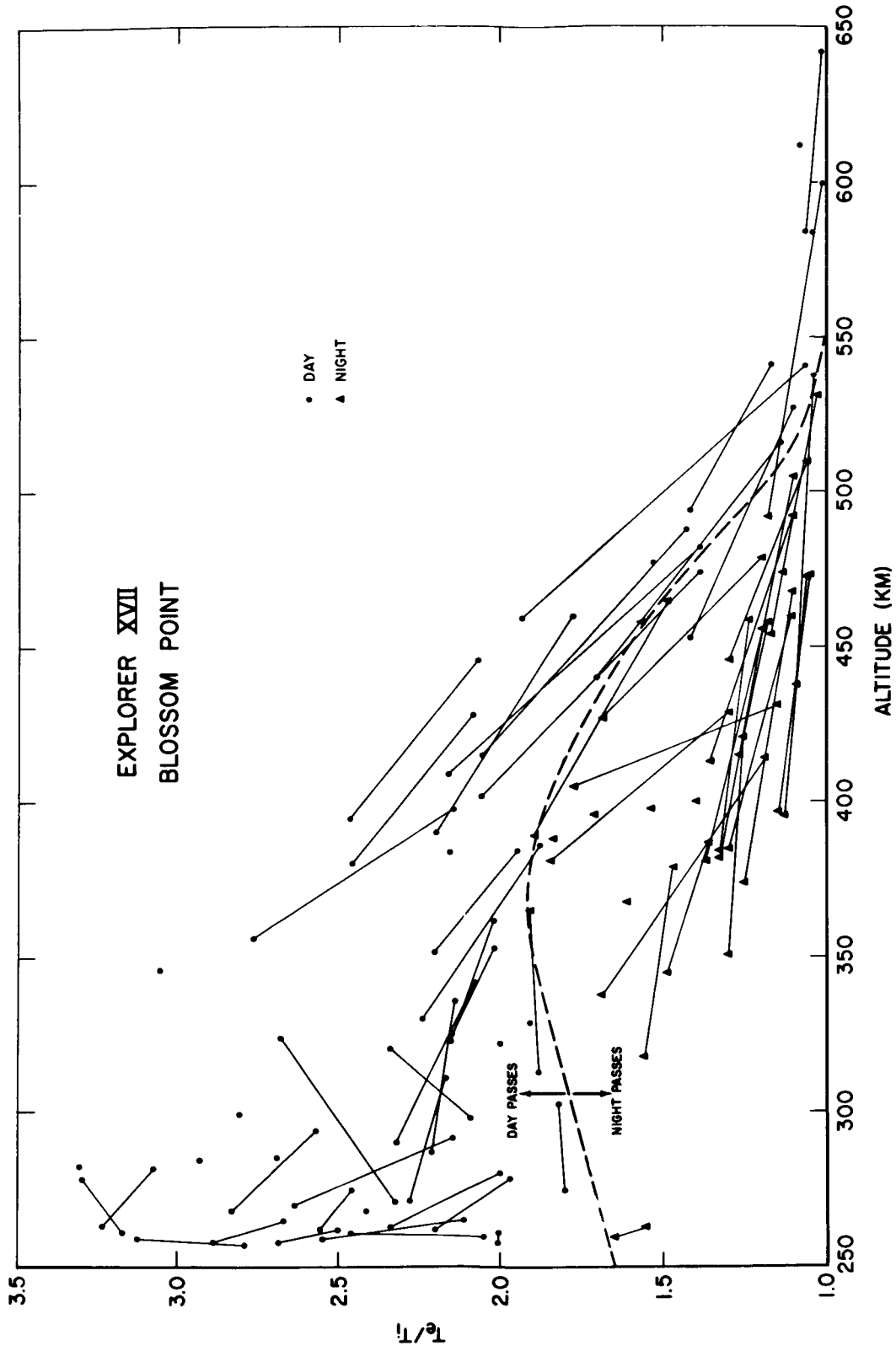
Figure 10—T_e/T_i at Blossom Point.

20

ELECTRON COOLING RATE vs T_e (at 250 km)
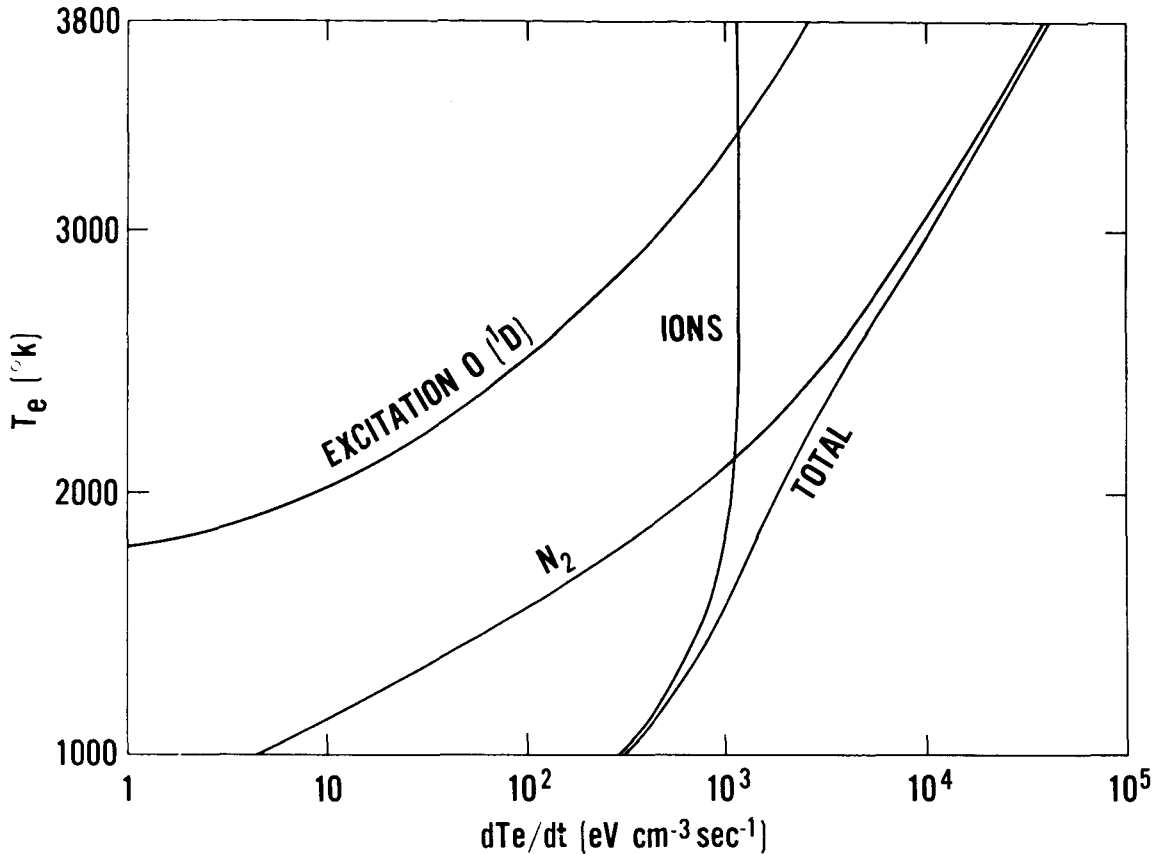
Figure 11—Electron Cooling Rates at 250 Kilometers Demonstrating
their Sensitivity to the Electron Temperature

adopted the model distributions of Harris and Priester (1962)[18] appropriate to
the local time of the measurement. The results for the southbound passes over
Blossom Point are shown in Figure 12 as a function of local time and altitude.
Local time effects dominate during the daytime southbound passes and it appears
that the heat input is roughly symmetrical about local noon, a variation in marked
contrast to the asymmetries in T_e and N_i. The heat input at 260 km has a max-
imum value of 4×10^3 eV cm^{-3} sec^{-1}. The nighttime values, presented in Fig-
ure 13, depend more strongly on altitude. They show clearly a non-vanishing
heat source decreasing with increasing altitude with a value of not less than 20 eV
cm^{-3} sec^{-1} at an altitude of 400 km. The importance of using calculated ion tem-
peratures is shown by a comparison of Figures 13 and 14. No clear pattern for Q
emerges from Figure 14, which is based upon the assumption that $T_i = T_g$.
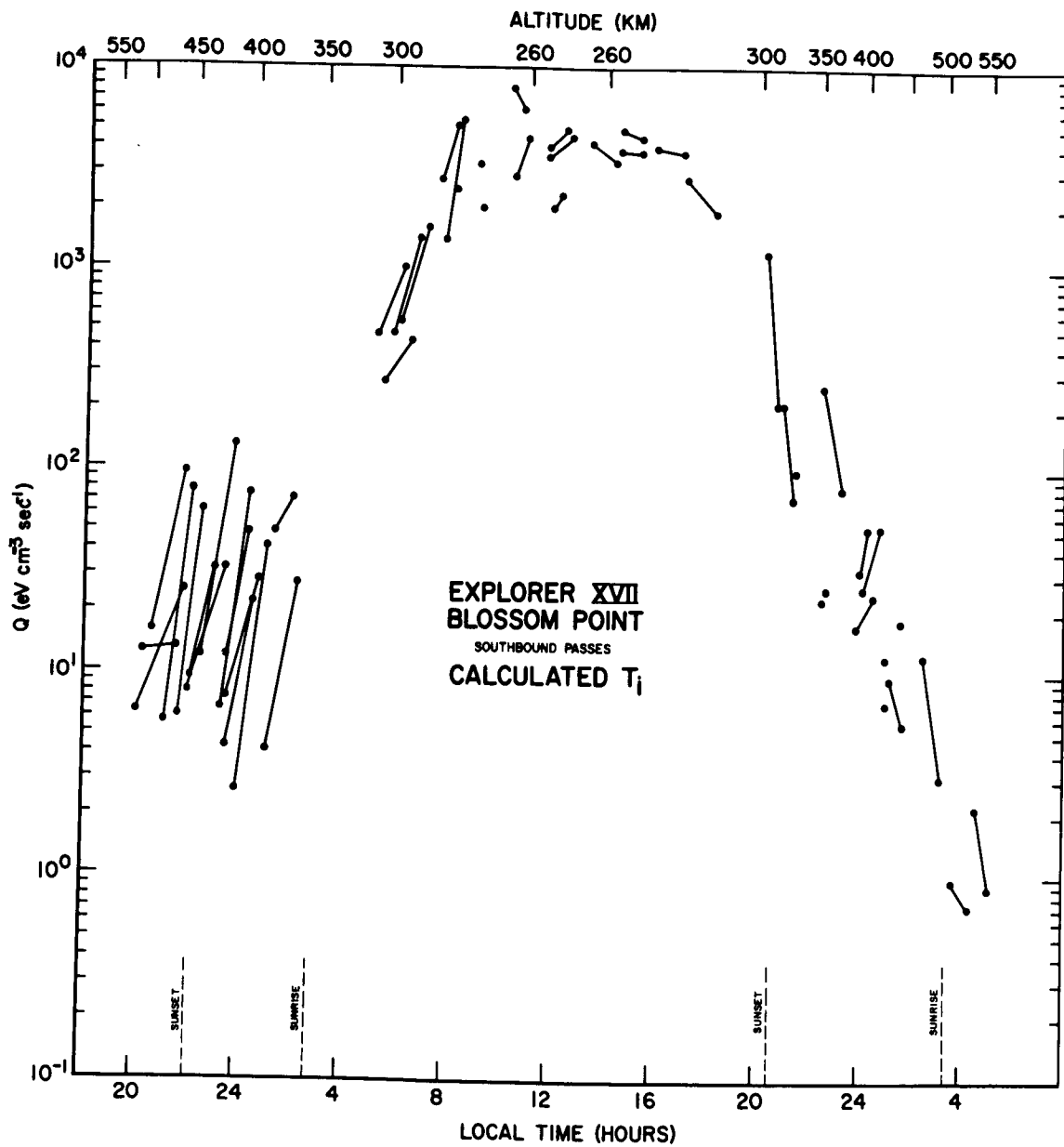
Figure 12—Locally Absorbed Energy (Q) Calculated for Southbound Passes. Local Time Effects Predominate in the Daylight Passes and Altitude Effects Control the Variations in the Nighttime Values of Q.
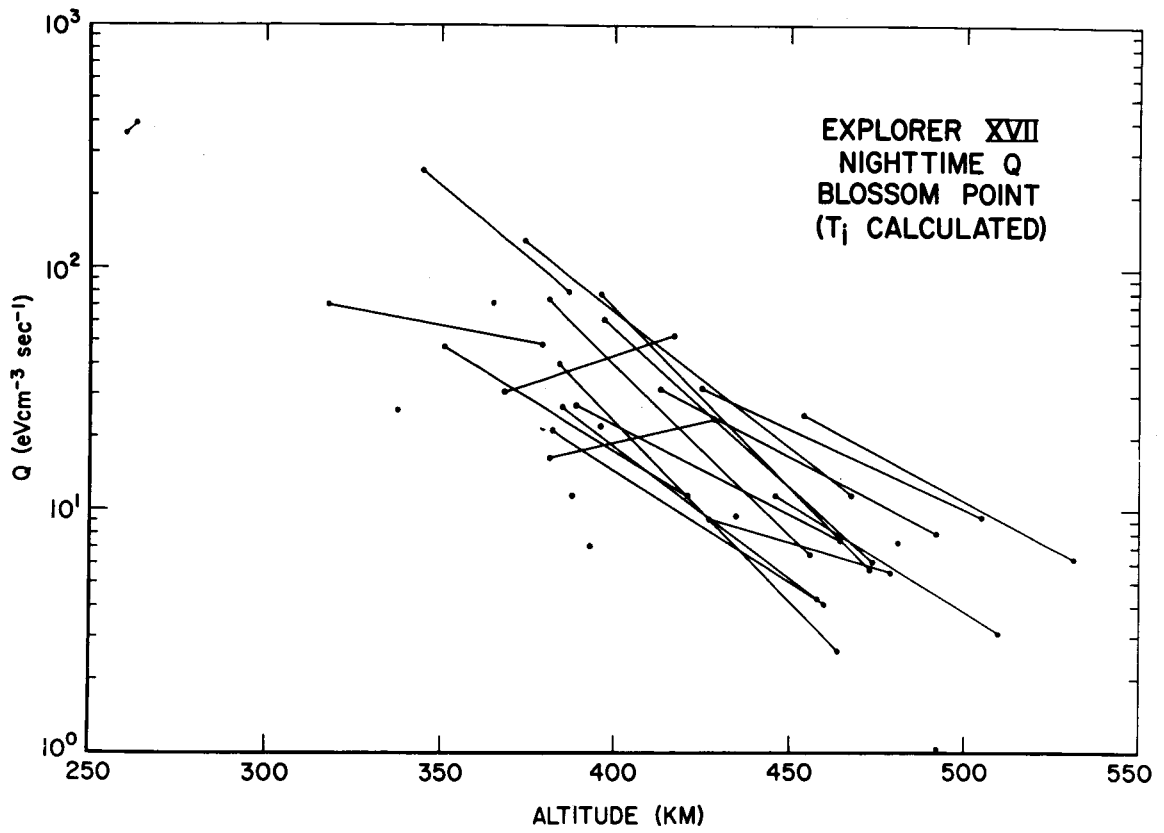
Figure 13—Q vs. Altitude in the Nighttime Ionosphere Using
the Calculated Values of T_i.
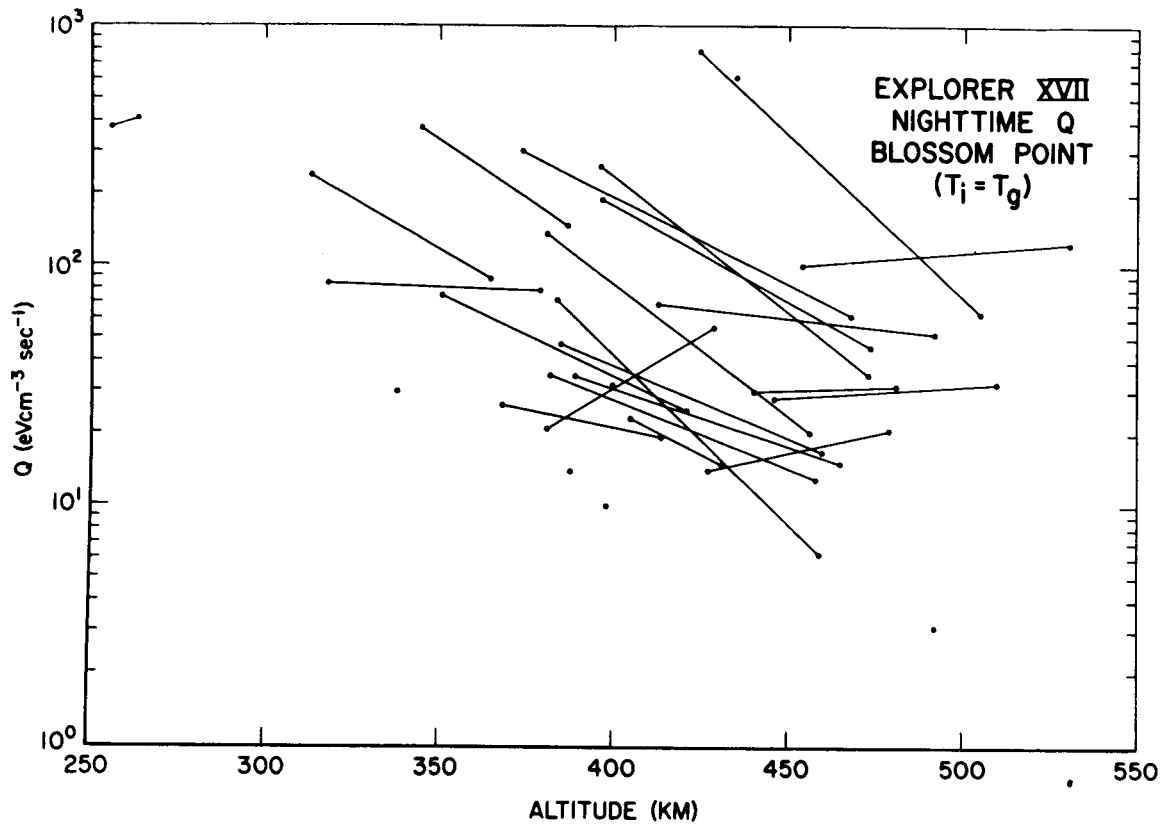
Figure 14-Q vs. Altitude in the Nighttime Ionosphere Assuming $T_i = T_g$. Note the Greater Scatter and Lack of Pattern Resulting from This Assumption.

The calculated values of Q for the northbound passes are shown in Figure 15. Local time and altitude effects are mixed and we have attempted to remove the dependence on local time by adopting for the northbound passes the diurnal variaation suggested by the southbound passes. The corrected values of Q, normalized to noon, are given in Figure 16. They show a heat input decreasing with altitude with an apparent change in the gradient in the region of 350 km.

DISCUSSION

The probe measurements of T_e from the Explorer XVII satellite confirm the conclusions of the rocket flights (Boggess, Brace and Spencer, 1959),[1] (Spencer, Brace and Carignan, 1962),[2] (Brace, Spencer and Carignan, 1963),[3] (Nagy, Brace, Carignan and Kanal, 1963)[24] that the difference between the temperature of the electrons in the F region of the ionosphere and the neutral particle temperature is large during the daytime and small but non-vanishing at night. These conclusions are in harmony with measurements on the Ariel satellite (Willmore, Henderson, Bowen and Boyd, 1964)[4] and on the Discoverer satellite (Sagalyn and Smiddy, 1964),[25] with observations of incoherent backscatter (Bowles, Ochs and Green, 1962),[26] (Evans, 1962),[27] (Pineo and Hynek, 1962),[28] (Evans, 1964),[19] (Evans and Lowenthal, 1964),[20] (Greenhow, Sutcliffe, Watkins)[21] and with a recent analysis of density profiles (Bauer, and Blumle, 1964).[30]

There are significant differences between the various data. In particular, Willmore, et al do not find the morning maximum in T_e which is a feature of the Explorer XVII data and which also appears in the backscatter observations of Evans and Loewenthal, the satellite data of Sagalyn and Smiddy and the density profile analysis of Bauer and Blumle. Bowles, et al, observing at the Equator, find a maximum at sunrise. As discussed earlier, Figure 8 shows that the time of the maximum depends at least partly upon geographic latitude.

Again in harmony with the rocket flight data, the Explorer XVII data show that T_e increases with latitude, a phenomenon also observed by Willmore, Henderson, Bowen and Boyd (1964).[4] The inverse relationship between T_e and n_e described in Equation (3) strongly suggests that the increase in T_e is caused by the decrease in n_e, a possibility noted by Dalgarno (1963).[8] The temperature may not continue to increase at high latitudes and a preliminary analysis of passes over Grand Forks at a latitude of approximately 65°N magnetic indicates that T_e had passed through a maximum (and n_e through a minimum).

Strong evidence that the positive ion temperature is also higher than the neutral particle temperature at altitudes above 300 km has been advanced by Evans (1964)[19] and by Evans and Loewenthal (1964)[20] and the averaged profiles of T_e and of T_e/T_i that they present are consistent with those given in Figures
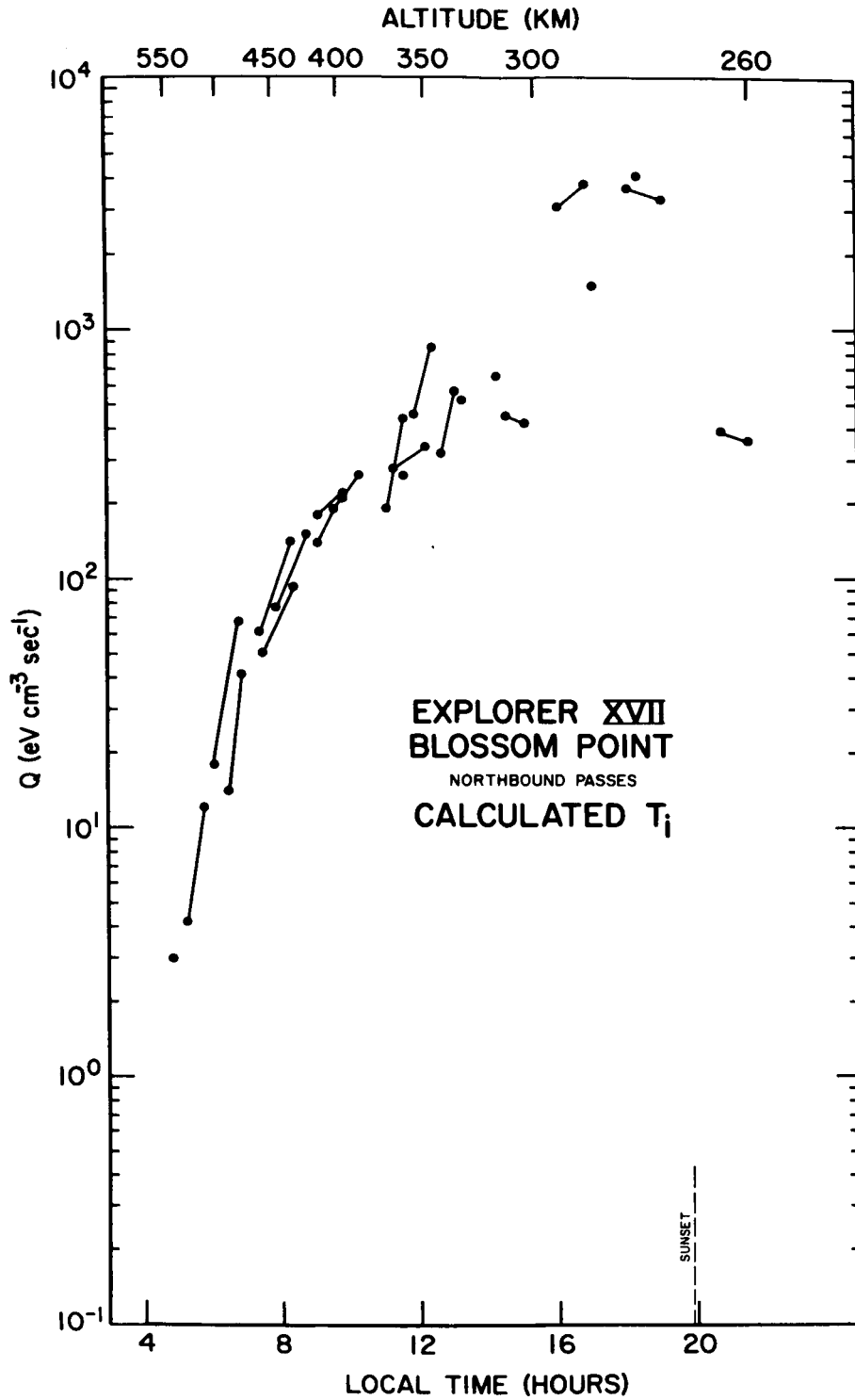
Figure 15—Q Calculated for Northbound Passes. Local Time and Altitude Effects are Strongly Mixed in These Passes, Particularly in the Early Morning.

Figure 16–Q vs. Altitude Normalized to Noon. This Altitude Variation of Q was Obtained from Northbound Passes by Removing the Diurnal Variation Suggested by Southbound Passes.

27
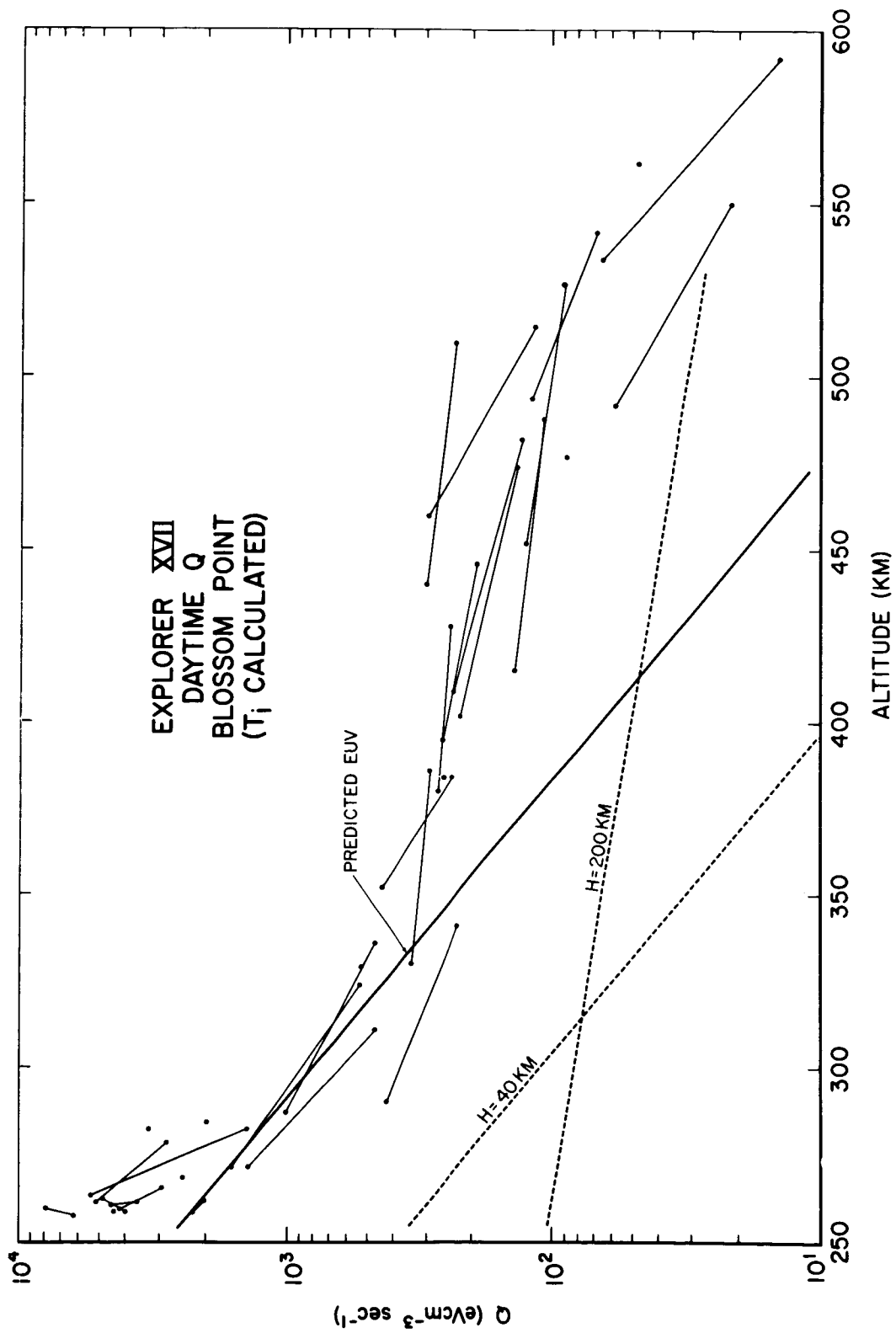
9 and 10, which are based upon Equation (8). The magnitudes of T_i at 400 km are in harmony with those measured by Boyd and Raitt (1964)[31] and it seems that over a considerable altitude extent $T_e > T_i > T_g$ with T_e/T_i approaching unity at high altitudes, a possibility to which Hanson (1963)[7] and Dalgarno (1963)[8] drew attention.

The heating effect of absorbed solar ultraviolet radiation has been investigated by Hanson and Johnson (1961),[5] by Dalgarno, McElroy and Moffett (1963),[6] by Hanson (1963)[7] and most recently by Dalgarno and McElroy (1964)[23] whose calculations make use of the improved photoionization calculations of Dalgarno, Henry, and Stewart (1964).[32] The assumption that the heat is deposited locally leads to the predicted euv heating shown in Figure 16, which is in agreement with the heating derived from the Explorer XVII measurements at altitudes below 300 km. Because of the escape of fast photoelectrons (Hanson, 1963)[7] the assumption of local heating is not valid above 300 km.

The gradient of the heat deposition from solar extreme ultraviolet radiation is equivalent to the neutral particle scale height, which is also shown in Figure 16 to emphasize the change in gradient near 350 km. This change in gradient demonstrates that absorption of energy by neutral particles is not the controlling process at great altitudes, and it suggests that the controlling process may be absorption by the ambient electrons, a typical gradient for which is also shown in Figure 16. Such a heat flux is to be expected at great altitudes from the escaping photoelectrons which lose energy by elastic collisions with the ambient electrons.

If j cm^{-2} sec^{-1} is the upward flux of photoelectrons and we adopt a mean of 10 eV for their energy, the rate of heating is given by

$$Q = 2 \, j \, n_e \times 10^{-13} \ eV \ cm^{-3} \ sec^{-1} \tag{9}$$

If the electrons cool by collisons with the positive ions O^+,

$$\frac{T_e - T_i}{T_e^{3/2}} = \frac{4 \times 10^{-7}}{n_e} \, j \, , \tag{10}$$

and if by collisons with He^+

$$\frac{T_e - T_i}{T_e^{3/2}} = \frac{1 \times 10^{-7}}{n_e} \, j \, . \tag{11}$$

28

It follows that an upward flux of about 5×10^8 cm^{-2} sec^{-1} may be sufficient to explain the Explorer XVII data, and it appears from the report of Hinteregger, Hall and Schmidtke (1964)[33] on the intensities of the extreme solar ultraviolet radiation, and from observations on Cosmos 3 and Cosmos 5 satellites (Mularchik and Vaisberg, 1964),[34] that such a flux is available.

Similar arguments have been advanced by Willmore (1964)[35] in a discussion of the Ariel measurements which were carried out a year earlier than Explorer XVII measurements, but which lead to daytime heat inputs smaller by a factor of two or three.

The fact that the electron temperature does not fall to the neutral particle temperature at night is of great interest, since it reveals the presence of an energy source in the nocturnal ionosphere. The heat input at an altitude of 400 km is about 20 eV cm^{-3} sec^{-1}, which is about five times larger than that derived from Ariel data. Willmore (1964)[35] has suggested that the energy source responsible for the Ariel observations can be identified with the fluxes of 2-3 kev electrons of about 8×10^9 cm^{-2} sec^{-1} observed by Vernon, Savenko, Shavrin, Nesterov, Pisivenko (1963).[36] This is an energy flux of 30 ergs cm^{-2} sec^{-1}, which is an order of magnitude larger than that of the solar ultraviolet radiation. If these electrons were precipitated into the atmosphere, they would give rise to 6 kilorayleighs of 3914 Å emission (c.f. Dalgarno, 1964)[37] whereas O'Brien, Allum and Goldwire (1964)[38] observe 5 rayleighs or less above 85 kilometers.

The difficulties presented by the large energy flux postulated by Willmore can be avoided by arbitrarily invoking instead a flux of soft electrons of, say, 100 eV energy. Assuming a heating efficiency of 0.1, the Ariel data require about 2×10^{-3} ergs cm^{-2} sec^{-1} and the Explorer XVII data require about 1×10^{-2} ergs cm^{-2} sec^{-4}. Fluxes of this order do not contradict any of the limits that have been derived from spectroscopic observations (c.f. Dalgarno, 1964)[37] and the resulting altitude variation in the heat deposition would be similar to that indicated by the data in Figure 16.

ACKNOWLEDGMENT

REFERENCES

1. Boggess, R.L., L.H. Brace, N.W. Spencer, J. Geophys. Res. 64, 1627 (1959)

2. Spencer, N.W., L.H. Brace, G.R. Carignan, J. Geophys. Res. 67, 157 (1962)

3. Brace, L.H., N.W. Spencer, G.R. Carignan, J. Geophys. Res. 68, 5397 (1963)

4. Bowen, P.J., R.L.F. Boyd, C.L. Henderson, A.P. Willmore, Proc. Roy. Soc. A, 281, 514 (1964)

5. Hanson, W.B., and F.S. Johnson, Mem. Soc. Sci. Liege, Series 5, 4, 390 (1961)

6. Dalgarno, A., M.B. McElroy and R.J. Moffett, Planet. Space Sci. 11, 463 (1963)

7. Hanson, W.B., Space Research III (North-Holland:Amsterdam) Edited by W. Priester (1963)

8. Dalgarno, A., National Aeronautics and Space Administration, CR-8 (1963)

9. Reber, C.A., and M. Nicolet, Planet. Space Sci. (in this issue) (1965)

10. Newton, G.P., R. Horowitz and W. Priester, Planet. Space Sci. (in this issue) (1965)

11. Brace, L.H., and N.W. Spencer, J. Geophys. Res. 69, (1964)

12. Mott-Smith, H.M., and I. Langmuir, Phys. Rev., 28, 727 (1926)

13. Spencer, N.W., Planet. Space Sci. (in this issue) (1965)

14. Spitzer, L., Physics of Fully Ionized Gases (Interscience, N.Y.) (1965)

15. Dalgarno, A., Phil. Trans. Roy. Soc., 250, 426 (1958)

16. Dalgarno, A., Annales de Geophysique, 17, 16 (1961)

17. Dalgarno, A., Journal of Atmos. and Terr. Phys., 26, 939 (1964)

18. Harris, I., and W. Priester, J. Geophys. Res., 67, 4585 (1962)

19. Evans, J.V., J. Geophys. Res., 69, 1436 (1964)

20. Evans, J.V., and M. Loewenthal, Planet. and Space Sci. 10, 905 (1964)

21. Noxon, J.F., J. Geophys. Res. 69, 3245 (1964)

22. Dalgarno, A., and J.C.G. Walker, Journ. Atmos. Sci., 21, 463 (1964)

23. Dalgarno, A., and M.B. McElroy, to be published (1964)

24. Nagy, A.F., L.H. Brace, G.R. Carignan and M. Kanal, J. Geophys. Res. 68, 6401 (1963)

25. Sagalyn, R.C., M. Smiddy, Y.N. Bhargava, presented at fifth International COSPAR meeting, Florence, (1964)

26. Bowles, K.L., E.R. Ochs, and J.L. Green, J. Res. NBS, 66, 395 (1962)

27. Evans, J.V., J. Geophys. Res., 67, 4914 (1962)

28. Pineo, V.C., D.P. Hynek, J. Geophys. Res. 67, 5119 (1962)

29. Greenhow, J.S., H.K. Sutcliffe and C.D. Watkins, Journ. Atmos. Terr. Phys., 25, 197 (1963)

30. Bauer, S.J., L. Blumle, J. Geophys. Res., 69, 3613 (1964)

31. Boyd, R.L.F., W.J. Raitt, to be published (1964)

32. Dalgarno, A., R.J.W. Henry, and A.L. Stewart, Planet. Space Sci. 12, 235 (1964)

33. Hinteregger, H.E., L.A. Hall, G.Schmidtke, presented at fifth International COSPAR meeting, Florence, (1964)

34. Mularchik, T.M., O.L. Vaisberg, presented at fifth International COSPAR meeting, Florence (1964)

35. Willmore, P.A., Proc. Roy. Soc. A, 281, 140 (1964)

36. Vernov, S.N., I.A. Savenko, P.I. Shavrin, V. YE Nesterov and N.F. Pisarenko, Planet. Space Sci., 11, 567 (1963)

37. Dalgarno, A., Annales de Geophysique, 20, 65 (1964)

38. O'Brien, B.J., R. Allum, and H.C. Goldwire, J. Geophys. Res. (submitted) (1964)